I&EC research
Industrial & Engineering Chemistry Research

pubs.acs.org/IECR
Article

Impact of Formulation of Photocurable Precursor Mixtures on the Performance and Dimensional Stability of Hierarchical Cation Exchange Membranes

Published as part of the Industrial & Engineering Chemistry Research virtual special issue "Membranes for Sustainability".

Daniel Firganek,* Mateusz L. Donten, and Bart Van der Bruggen

Cite This: https://doi.org/10.1021/acs.iecr.3c02174

ABSTRACT: This work presents a systematic approach to formulating UV curable ionomer coatings that can be used as ion-exchange membranes when they are applied on porous substrates. Ion-exchange membranes fabricated in this way can be a cost-effective alternative to perfluorosulfonic acid membranes, such as Nafion and similar thin ionomer film membranes. Hierarchically structured coated membranes find applications for energy storage and conversion (organic redox flow batteries and artificial photosynthesis cells) and separation processes (electrodialysis). Designing the ionomer precursor for membrane formulation requires the introduction of compounds with drastically different properties into a liquid mixture. Hansen solubility theory was used to find the solvents to compatibilize main formulation components: acrylic sulfone salt (3-sulfopropyl methacrylate potassium salt) and hexafunctional polyester acrylate cross-linker (Ebecryl 830), otherwise nonmiscible or mutely soluble. Among the identified suitable solvents, acrylic acid and acetic acid allowed for optimal mixing of the components and reaching the highest levels of sulfonic group content, providing the desired ion-exchange capacity. Interestingly, they represented a case of a reactive and nonreactive solvent since acrylic acid was built into the ionomer during the UV curing step. Properties of the two membrane variants were compared. Samples fabricated with acetic acid exhibit improved handleability compared with the case of acrylic acid. Acetic acid yielded a lower area-specific resistance (6.4 ± 0.17 Ohm·cm^2) compared to acrylic acid (12.1 ± 0.16 Ohm·cm^2 in 0.5 M NaCl). This was achieved without severely suppressing the selectivity of the membrane, which was standing at 93.4 and 96.4% for preparation with acetic and acrylic acid, respectively.

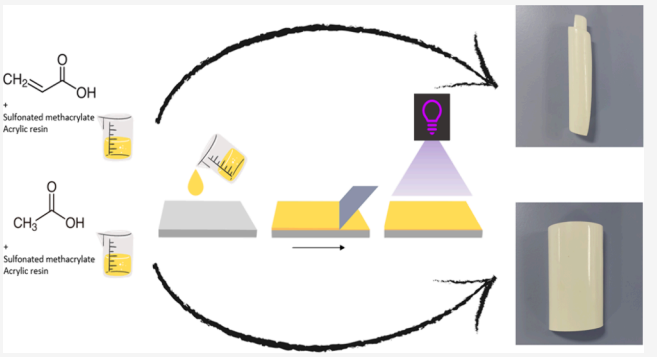

1. INTRODUCTION

Membrane technologies have been gaining interest over the last few decades and find numerous applications, displacing traditional systems, being more sustainable by offering higher efficiencies at lower cost.[1,2] Ion-exchange membranes (IEMs) are widely used in fields such as water purification and demineralization,[3] resource recovery,[4] energy storage,[5] and energy conversion,[6] to name just a few of the many. Due to the current strive to neutrality for the environment, great effort in technology development is being put to lower the material cost, reduce the use of resources, and limit waste disposal.[7] Following these trends, many ion-exchange membrane concepts emerged as an alternative for perfluorosulfonic acid membranes such as Nafion, which have been extensively used in many applications.[8,9] The high cost of perfluorinated membranes and other common homogeneous ion-exchange membranes is largely due to the energy- and resource-intensive fabrication process. Additionally, many industrial fabrication processes of homogeneous membranes require the use of harsh chemicals such as *N*-methyl-2-pyrrolidone (NMP), *N*,*N*-dimethylacetamide, and *N*,*N*-dimethylformamide. Membrane manufacturing is often followed by excessive waste generation due to the disposal of residual chemicals in the environment.[10,11] The membrane industry is estimated to contribute to the generation of wastewater in an amount exceeding 50 billion liters every year.[12] Hence, heterogeneous membranes were proposed as they offer good performance at a much lower cost than homogeneous IEMs. Heterogeneous membranes are

Received: June 28, 2023
Revised: September 7, 2023
Accepted: September 12, 2023

composite materials in which the two phases, the ion exchange material and the structural polymer, are well distinguishable. The vast majority of membranes of this type are manufactured by blending the ion-exchange resin with an inert polymer binder. This structure gives more freedom in choosing materials for membrane fabrication as the two phases can complement each other with respect to the desired properties; this is different from single-phase homogeneous membranes.[13] On the other hand, the two-phase blend of heterogeneous membranes causes deterioration of some properties due to imperfections in the membrane structure such as interstitial free water volume, which gives additional pathways for ions and thus loss of ionic selectivity. Nevertheless, over recent years, the development of heterogeneous membranes led to an improvement of membrane properties allowing for better cost-effectiveness of such a membrane concept.[14]

Hierarchical ion-exchange membranes (hIEMs) are a particularly interesting membrane type in which the functions of ion transport and mechanical robustness are decoupled into two distinct layers.[15] The hierarchical membrane concept assumes the coexistence of a thin (usually from 20 to 50 μm) coating layer composed of a functionalized polymer and a robust, often thick (within hundreds of micrometers) supporting layer made of a mechanically and dimensionally stable porous material. In such an arrangement, the functional coating layer governs the ion-exchange properties of a membrane, while the mechanical strength is granted by the supporting layer.[16−18] hIEMs offer several advantages, for example, a competitive performance at lower fabrication and material cost and over perfluorinated membranes due to the simpler and less energy-intensive production process. One of the aspects limiting the widespread use of hIEMs in membrane technologies is the concentration polarization. Due to different kinetics of transport of ions in the solution and in the membrane, a depletion layer and an enrichment layer emerge next to the membrane surface. The rise of this concentration profile compromises the separation efficiency of the membrane.[19] In the case of hierarchical membranes, the concentration polarization is more severe on the porous support side due to inadequate mixing.

A hierarchical structure allows for some freedom in material development typical for heterogeneous membranes: the optimization of mechanical properties and ion-exchange performance can be undertaken independently by the selection of two different materials independently. As the mechanical properties of the composite membrane are governed by the supporting layer, the ion-exchange performance of the membrane can be tuned by the selection of monomers which form an ionomer of a structure that normally would not possess mechanical properties to form a self-supported membrane.[20] The UV curing employed in the fabrication of ionomer coatings leads to the shrinkage of the coating layer when the liquid formulation of monomers hardens under UV exposure. Ionomers formed by the radical polymerization of sulfonated low-molecular-weight functional monomers with cross-linkers such as, for example, divinylbenzene (DVB), are prone to shrinkage since the dense and highly cross-linked polymer network is formed. The swelling behavior of the DVB copolymers when exposed to aqueous solutions leads to dimensional changes, which can affect the physical integrity of the polymer.[21] High-molecular-weight multifunctional acrylic resins can be used as cross-linkers for UV curable coatings since the shrinkage rate can be limited by increasing the molecular volume of the cross-linker.[22] In a previous work of our group, a chemistry platform for the fabrication of UV-cured hIEMs was developed.[23] In this concept, UV-reactive acrylic precursors were formulated into a liquid mixture and cured to form a dense ion-exchange layer on top of a porous substrate. Due to their hierarchical structure, these membranes have a tendency for mechanical deformations, for example, curling up when hydrated.[24] The reason for this is a discrepancy in expansion coefficients between the coating layer and the supporting layer under wetting. The supporting layer is a robust material with well-defined pore size that do not expand upon wetting as water molecules are filling only the free volume of the material.[16] On the other hand, ion-exchange coatings have a tendency to change in dimensions when turning from a dry to wet state. The coating in the dry state is a homogeneous dense material without any pores. Hydration of the ionomer coating layer causes the formation of hydrophilic channels when the charged functional groups of the ionomer are solvated with water molecules. The size and shape of these channels are not well-defined and depend on the degree of swelling and cross-linking network of the ionomer.[25] As the coating is dimensionally confined by the supporting layer, the stress that arises as a result of expansion of the coating layer leads to the mechanical deformation of the entire membrane. Excessive ionomer swelling compromises the mechanical properties and leads to difficulties in handling the membrane, which can cause handling difficulties or operation failure. The use of a fully UV-reactive formulation in hIEM development leads to intensive swelling as the formation of water channels strongly affects the structure of the coating. The reason for this is that the water channels are formed within the highly cross-linked dense structure of the UV-hardened ionomer layer. As a consequence, the ionomer coating is undergoing a significant volumetric expansion upon contact with aqueous electrolyte.[23] In this case, excessive mechanical deformation is posing serious difficulties in handling the membrane in a cell assembly (e.g., ED stack). Moreover, the progressive swell of a coating when a membrane is placed in a fixed position in a cell may cause crack of the membrane due to the internal stress arisen.[26] Composite hIEMs were previously developed and fabricated with the use of a non-UV-reactive solvent in membrane formulation.[16,17] It was proposed that the introduction of a nonreactive solvent to the UV-reactive acrylic precursor mixture allows for the preparation of an ionomer matrix initially swollen by the solvent, limiting the expansion of the coating in contact with water. However, a proper solvent selection for membrane formulation is a challenge since ionomer precursors often reveal drastically different solvation properties.

In this work, a systematic approach utilizing Hansen solubility theory was used in order to find a suitable solvent to compatibilize two main formulation components for the fabrication of hierarchical cation-exchange membranes. The Hansen solubility parameter (HSP) was introduced by Dr. Charles Hansen based on the Hildebrand theory, which defines the solubility parameter of a solvent as the square root of the cohesive energy density.[27] The HSPs can be measured experimentally, and up to now HSPs were determined and reported for more than 1300 common solvents.[28]

Herein, we report the formulation and fabrication of a UV-curable cation-exchange membrane with good handleability and mechanical stability. While the miscibility of membrane formulation components with a solvent can be predicted by the

https://doi.org/10.1021/acs.iecr.3c02174
Ind. Eng. Chem. Res. XXXX, XXX, XXX−XXX

model based on HSPs, the maximum solubility of the components in a given solvent needs to be assessed.[29] The high load of functional monomer in the formulation is essential to reach a high concentration of ion-exchange groups in the polymer matrix, and the solubility of a cross-linker defines the limit of the cross-linking density. The high number of ion-exchange groups provides a good ion-transport performance, while the cross-linking density is crucial for the membrane selectivity and limiting transport of uncharged molecules such as, for example, alcohols.[30] Some margin for extra solvency of formulation components is advised to avoid phase separation due to temperature variations and so forth during the membrane fabrication process.[28] The good compatibility of a solvent with other formulation components is necessary to allow for reaching an optimal functional-cross-linker content ratio and thus tuning the membrane properties.[31,32] Last but not the least, the suitability of the solvent for the membrane formulation should be evaluated by taking into account the reduction of economic and environmental costs.[29] The physical, chemical, and electrochemical properties of the membranes formulated and fabricated with the most promising solvents were measured and benchmarked against hIEM preparation with acrylic acid (AA-hIEM) reported previously by Deboli et al.,[23] as well as against commercial heterogeneous and homogeneous cation-exchange membranes.[33−35]

2. EXPERIMENTAL SECTION

2.1. Materials and Chemicals. Ebecryl 830 (Ebe830) hexa-functional polyester acrylate oligomer was received as a sample from Allnex S.A./N.V. (Belgium); 3-sulfopropyl methacrylate potassium salt (SPMA) was purchased from TCI Co., Ltd. (Japan). Ethyl l-lactate (EtL), dipropylene glycol (DPG), propan-2-ol, chloroform, and triethylamine were purchased from Alfa Aesar (United States). Acrylic acid (AA), dichloromethane, methyl methacrylate, 4-vinylpyridine, 1-vinyl-2-pyrrolidone, 2-methyl-2-butanol, 2-ethyl-1-hexanol, acetone, allylamine, cyclohexanone, diethylene glycol methyl ether, dimethyl sulfoxide, ethylenediamine, hexane, methanol, *N*-methyl-2-pyrrolidone, propan-2-ol, polyvinylpyrrolidone K 90 (PVP), styrene, and DVB were ordered from Merck GmbH (Germany). Acetic acid (AcA) was purchased from POCH z.o.o. (Poland). Sodium chloride, toluene, acetonitrile, tetrahydrofuran, 1-methyl-2-pyrrolidone, and ultrapure water were purchased from Chem-Lab N.V. (Belgium). Ethylenediamine was obtained from Fisher Scientific (United States), and diphenyl(2,4,6-trimethylbenzoyl) phosphine oxide (TPO) was purchased from Hock GmbH (Germany). The standard homogeneous cation-exchange membrane Nafion 117 was provided by Dupont (United States). Ralex CMHPES from MEGA A.S. (Czech Republic) and FKS-PET-75 from Fumatech GmbH (Germany) were used as heterogeneous cation-exchange membrane benchmarks.

2.2. PVC-SiO_2 Porous Supporting Membrane. The PVC-SiO_2 support was produced internally at Amer-Sil S.A. (Luxembourg) following the process described in patent US8039140B237. The PVC-SiO_2 support material is an ultrafiltration membrane with the 60.3 nm median pore size. The porosity of the PVC-SiO_2 membrane equals 1.034 $cm^3 \cdot g^{-1}$, and the volume porosity reaches 64.8%. The moderate hydrophilicity of the ion-exchange coating formulation assures good compatibility with the substrate and determines good adhesion of the coating on the supporting membrane. The good adhesion of the ion-exchange layer on the substrate is secured due to the penetration of the pores on the support surface by the ion-exchange formulation during the coating process. On the contrary, developed ion-exchange formulations show poor adhesion on hydrophobic supporting membranes such as, for example, PTFE, and the resulting coatings delaminate easily from the support. The impregnation of the substrate by the ion-exchange formulation can be avoided, for example, by controlling the viscosity of the formulation.

2.3. Hansen Solubility. According to the Hansen solubility theory, the total cohesive energy can be split into three separate contributions: (1) dispersion, (2) dipole−dipole, and (3) hydrogen bonding interactions. The three individual cohesive energy components represented by the δ_D, δ_P, and δ_H parameters make up the total Hansen solubility δ^2 (eq 1).

$$\delta^2 = {\delta_D}^2 + {\delta_P}^2 + {\delta_H}^2 \quad (1)$$

By plotting the HSP of the good and bad solvents for a given solute in a 3D Hansen space, the solubility domain of the solute can be determined. The solubility domain is defined by dispersion δ_D, polar δ_P, and hydrogen bonding δ_H parameters, being the coordinates of a center of the sphere, with the so-called interaction radius R_0 of that sphere. A mathematical algorithm was proposed to minimize the interaction radius (R_0) in such a way that all good solvents exist within the sphere and bad solvents are outside the sphere.[36]

To determine the HSPs of both analytes, 3-sulfopropyl methacrylate potassium salt and hexa-functional polyester acrylate oligomer Ebecryl 830, a set of solutions containing ca. 5% (w/w) of each analyte were prepared in 25 screening solvents. The samples were thoroughly shaken and left for 48 h to equilibrate. Then, each sample was visually checked to see whether the analyte was dissolved or not. The good and bad solvents for SPMA and Ebe830 were identified and listed (Table S.1, Supporting Information). The HSP parameters for SPMA and Ebe830 were calculated, and the interaction radius (R_0) was estimated according to the fitting model introduced by Díaz de los Ríos et al. with use of Microsoft Excel software.[36]

The four parameters (dispersion parameter, polar parameter, hydrogen bonding parameter, and interaction radius) define the solubility domain of the analyte in a 3D Hansen space. The model is estimating the R_0 values based on the best fit where experimentally identified good solvents are inside the calculated solubility domain and bad solvents are outside the solubility domain of an analyte. For optimal mixing, the relative energy difference (RED) between the solvent and solute should be as small as possible. The RED can be expressed as a ratio (eq 2):

$$\mathrm{RED} = \frac{R_a}{R_0} \quad (2)$$

where R_a is the distance between HSP of the solvent and the solute in the 3D Hansen space (eq 3) and R_0 is the interaction radius.

$$R_a = \sqrt{4(\delta_{D2} - \delta_{D1})^2 + (\delta_{P2} - \delta_{P1})^2 + (\delta_{H2} - \delta_{H1})^2} \quad (3)$$

According to Hansen theory, the good solvents are indicated by RED $\leq$ 1.

2.4. Membrane Preparation. Membranes were fabricated in a three-step process utilizing a blade coating and UV curing.

https://doi.org/10.1021/acs.iecr.3c02174
Ind. Eng. Chem. Res. XXXX, XXX, XXX−XXX

This fabrication methodology was successfully applied and reported in previous work of our group.[16,17,23] In the first step of membrane fabrication, the ionomer precursor mixture is formulated. SPMA is dissolved in a given solvent by sonication at 40 °C for 2 h. The SPMA concentrations and solvents are reported (Figure 2) in Section 3.2 where optimal solvent selection for membrane formulations is discussed. PVP was added to the SPMA solution of low viscosity and sonicated until a homogeneous solution was obtained (40 °C, 2 h). Ebecryl 830 resin and TPO photoinitiator were then added, and the mixture was thoroughly stirred. The resulted mixture was sonicated for 20 min at 40 °C to remove air bubbles and left for another 20 min at room temperature. The final formulation compositions are summarized in Section 3.2, Figure 2. Subsequently, liquid formulation is spread on a porous PVC-silica supporting membrane by a cylindrical blade with 90 μm gap mounted on an automatic applicator (BYK GmbH, Germany). In the last step, the formulation undergoes radical polymerization reaction in a UV conveyor (Jenton International Ltd., United Kingdom) under irradiation by a 200 W iron-doped mercury lamp (λ = 365 nm). Before electrochemical and permeation experiments, the membranes were activated in an electrolyte solution for at least 48 h and rinsed with deionized (DI) water.

2.5. Water Uptake. The water uptake (WU) of the hIEM was determined by means of the water weight content in a fully hydrated ion-exchange coating without a porous PVC-silica support. WU was calculated according to eq 4.

$$\mathrm{WU}[\%] = \frac{m_w - m_d}{m_d} \times 100\% \tag{4}$$

where m_w and m_d [g] are the mass of hydrated and dry membranes, respectively.

Each sample was prepared by curing the ionomer precursor formulation on Teflon according to the procedure described in Section 2.4. The resulting ion-exchange material was peeled off the Teflon substrate and immersed in 0.5 M NaCl aqueous solution for 48 h to turn the ionomer into Na^+ form and wash all unreacted species. Subsequently, each sample was immersed in DI water for 24 h, wiped with absorbent paper in order to remove water from the sample surface, and weighted on an analytical balance (m_w). To obtain the dry mass of the sample (m_d), the samples were weighed after drying in an oven at 80 °C for 48 h.

2.6. Elemental Analysis of Sulfur. The quantification of sulfur in ion-exchange coatings was performed by a FlashSmart Elemental Analyzer (Thermo Fisher, USA) equipped with a thermal conductivity detector. The combustion temperature was 900 °C.

2.7. Ion-Exchange Capacity. The ion-exchange capacity (IEC) of the ion-exchange functional coatings was determined experimentally by titration. Samples of the coating material were weighted and equilibrized in 0.5 M NaCl solution for 72 h, replacing the solution with a fresh one every 24 h. The equilibration was done in order to wash out the solvent and residual unreacted species and transfer the samples into the Na^+ form. The samples were then rinsed with ultrapure water, and the excess water was then removed with adsorbent paper. In the next step, samples were placed in 100 mL of 0.05 M HCl for 48 h to exchange Na^+ counterions of the ionomer into H^+ form. The change of the H^+ concentration in the solution was then determined by titration with 0.1 M NaOH, and the IEC was calculated (eq 5).

$$\mathrm{IEC}_{exp}\ [\mathrm{mmol \cdot g^{-1}}] = \frac{(V_0 - V_s)c_{NaOH}}{m} \tag{5}$$

where V_0 and V_s [dm^3] are the volumes of NaOH solution used to titrate the HCl solution before and after equilibration with the sample, respectively. c_{NaOH} [$mmol \cdot dm^{-3}$] denotes the concentration of the titrant, and m [g] is the mass of the sample of coating material.

To ensure that the replacement of Na^+ ions with H^+ ions was complete, membrane samples were rinsed with ultrapure water, wiped with adsorbent paper, and immersed in fresh portion of 0.05 M HCl for another 48 h. The changes of the H^+ concentration in the solution and IEC were determined as described above. The equilibration of coating flakes in 0.05 M HCl was repeated until the consumption of H^+ by the membrane samples was not observed. At this point, the replacement of Na^+ ions by H^+ ions is considered completed. The IEC values reported in Section 3.3 are cumulative IEC values calculated from the total H^+ consumption at each step of equilibration. The obtained IEC values at each equilibration step are averaged from two measurements.

2.8. Area-Specific Resistance. The area-specific resistance (ASR) of the membrane was determined by utilizing a custom-designed electrochemical cell with a four-electrode configuration. This method was already reported elsewhere.[16,23] Briefly, each membrane was activated in 0.5 M NaCl solution for no less than 48 h before placing in the clamps, determining the 19.63 cm^2 effective active area of the membrane, and mounted in the cell filled with 0.5 M NaCl solution. The temperature of the solution was kept at 25 °C during the measurement, and the voltage drop between two saturated calomel electrodes placed on both sides of the membrane was recorded while applying the current from 0 to 100 mA at a 5 mA/s scan rate. The resistance is expressed by the slope of the resulting polarization curve. The membrane resistance was calculated according to eq 6.

$$R[\Omega \cdot \mathrm{cm^2}] = (R_m - R_0) \cdot A \tag{6}$$

where R_m and R_0 [Ω] are the measured resistance with and without the membrane, respectively. A [cm^2] is the active area of the membrane.

2.9. Membrane Selectivity. The selectivity of the membrane was determined by potentiometric measurement in a custom-made cell consisting of two half-cells separated by the membrane with a 19.63 cm^2 exposed active area. Membrane samples were equilibrated in a 0.1 M KCl solution for 48 h before the measurement. Both half-cells were equipped with saturated calomel electrodes and filled with KCl aqueous solutions of 0.5 and 0.1 M on the two sides of the membrane to create membrane polarization. The temperature of the solution was monitored, and the potential difference between calomel electrodes was measured for around 10 min until a stable value was obtained. The data collected were used to calculate the membrane selectivity.

Data processing followed the approach taken by Wilhelm et al.[37] and Długołęcki et al.[38] The theoretical potential value that would be reached for a 100% selective membrane (E_{th}) was calculated from the Nernst equation (eq 7). This number was compared with the potential recorded in the experiment (E_m), and selectivity was expressed in percentage (eq 8). For assuring accuracy, corrections were made to offset the experimental results by any potential difference between the two electrodes. This value was determined by placing both electrodes in 0.5 M

https://doi.org/10.1021/acs.iecr.3c02174
Ind. Eng. Chem. Res. XXXX, XXX, XXX−XXX

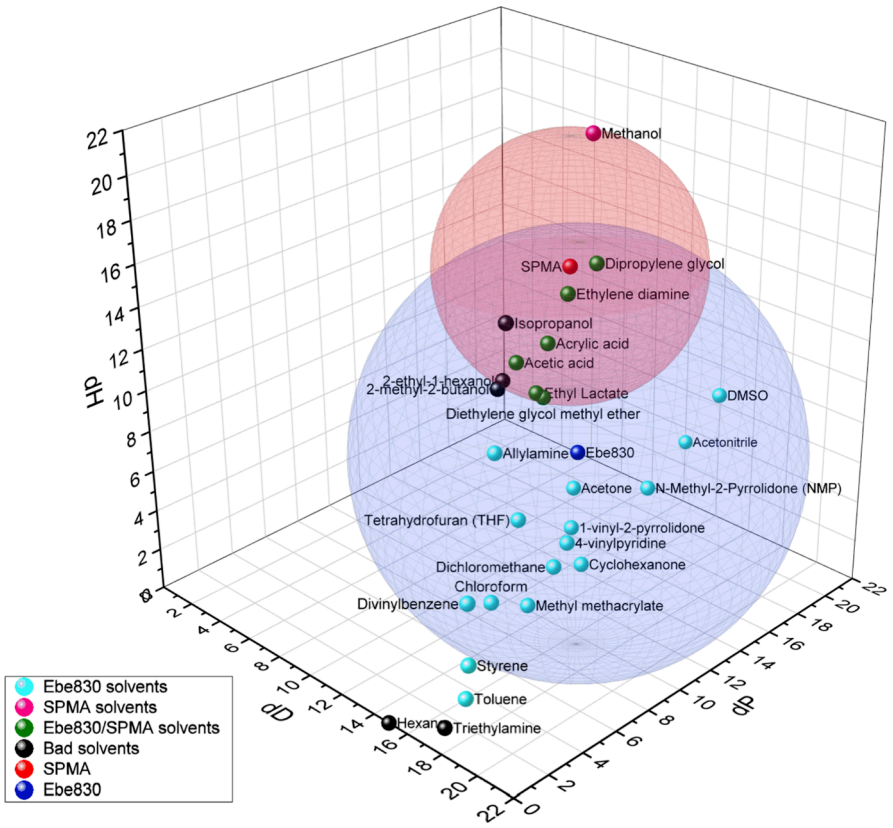

Figure 1. SPMA and Ebe830 solubility domains in the 3D Hansen space.

KCl solution, conditions under which 0 mV reading was expected; the value read was used to offset all experimental data.

Cha et al.[39] and Kingsbury et al.[40] report on the interference of junction potential of reference electrodes used in such measurements. For assuring consistency with the vast literature on IEM,[10,41−45] such corrections were not applied to the data presented. The junction potential for the experimental setup resulting from two saturated calomel electrodes immersed in 0.5 and 0.1 M KCl solutions was calculated and described in the Supporting Information. Their impact was however found not to affect the conclusions on the overall performance of the membranes as it leads to shift of all selectivity values including that of the benchmark.

$$E_{th}[V] = \frac{RT}{F}\ln\frac{f_1 \cdot c_1}{f_2 \cdot c_2} \tag{7}$$

where R is the gas constant $[J \cdot mol^{-1} \cdot K^{-1}]$, T [K] is the temperature, F $[C \cdot mol^{-1}]$ is the Faraday constant (F = 96,485 C/mol), and f_1 and f_2 represent the activity coefficients of 0.5 and 0.1 M KCl solutions, respectively. The concentration of each KCl solution is denoted as c [M].

The membrane selectivity was expressed by the ratio of the measured membrane potential (E_m) and the theoretical potential (E_{th}) (eq 8):

$$\alpha[\%] = \frac{E_m}{E_{th}} \times 100\% \tag{8}$$

where E_m [V] is the measured membrane potential and E_{th} [V] is the theoretical membrane potential.

2.10. Permeability of Ethanol. The permeation experiment was performed in a custom-designed diffusion cell composed of two chambers. The tested membrane was activated in 0.5 M NaCl solution for 24 h and thoroughly rinsed with DI water. Subsequently, the membrane sample was placed in between the two chambers with 15.90 cm^2 of exposed effective area and tightly clamped. The donor half-cell was filled with 300 mL of 1 M ethanol solution, and 300 mL of ultrapure water was added to the receiving half-cell. The concentration evolution of ethanol in the receiving cell was observed by sampling the solution over time and measuring the ethanol concentration via gas chromatography (Clarus 500 Gas Chromatograph, PerkinElmer, United States). The permeability parameter was calculated from the linearized fit of eq 9. In the case of coated membranes, there is an additional ambiguity regarding the proper quantification of the membrane thickness. To mitigate that differentiation, normalization to thickness was not performed and permeability parameters were expressed in $[cm \cdot min^{-1}]$ which is a value in reference to a sheet of membrane, regardless of its thickness (eq 11). In practice, for easy linearization of eq 9, permeability experiments need to follow the assumptions of nearly constant concentration of the solution in the donor cell over time.

$$\ln\left(\frac{c_A}{c_A - c_B}\right) = \frac{DA}{V_B L} \times t \tag{9}$$

$$D\left[\frac{cm^2}{min}\right] = a \times \frac{V_B L}{A} \tag{10}$$

https://doi.org/10.1021/acs.iecr.3c02174
Ind. Eng. Chem. Res. XXXX, XXX, XXX−XXX

$$D\left[\frac{\text{cm}}{\text{min}}\right] = a \times \frac{V_B}{A} \tag{11}$$

where D is the permeability parameter and c_A and c_B are the concentrations in the donor and receiving solutions [mol·dm^{-3}], respectively. A is the exposed area of the membrane [cm^2], V_B is the volume of solution in the donor cell [cm^3], L is the thickness of the membrane [cm], and t is the time [min].

2.11. Osmotic Water Permeation. The water permeation coefficient (WPC) was measured in a two-compartment diffusion cell with 19.63 cm^2 exposed membrane area. The membrane sample was activated in 0.5 M NaCl solution for 48 h, thoroughly rinsed with DI water and clamped between the two compartments of the diffusion cell. One side of the cell was filled with 190 mL of 4 M NaCl solution, while the second was filled with 190 mL of DI water. Solutions in both compartments were stirred and the change in volume in the high concentration compartment was recorded after 20 h. The water permeation coefficient was calculated according to eq 12:[46]

$$\frac{D_w}{d}[\text{cm}^4\ \text{s}^{-1}\ \text{mol}^{-1}] = \frac{\Delta V \times 10^3}{\Delta C t A} \tag{12}$$

where ΔV is the volume change in the high concentration compartment [cm^3], ΔC is the concentration gradient between the two compartments [mol·dm^{-3}], t is the experiment duration [s], and A is the membrane active area [cm^2].

The water permeation coefficient was determined with the assumption that the concentration of the salt in the high concentration remains constant over the experimental time.

3. RESULTS AND DISCUSSION

3.1. Solvent Selection. Figure 1 is a graphical representation of the results of the SPMA and Ebe830 solubility interaction sphere determination and solvent assessment. The red sphere (δ_D = 15.55, δ_P = 10.05, δ_H = 17.45, and R_0 = 5.60) and blue sphere (δ_D = 16.55, δ_P = 9.50, δ_H = 9.50, and R_0 = 9.50) represent SPMA and Ebe830, respectively. Light blue solid points represent experimentally assessed good solvents for Ebe830, and light red points indicate good solvents for SPMA. Black points represent the bad solvents for both analytes. Green points represent solvents that were experimentally proven to dissolve both SPMA and Ebe830 together with the solvents predicted by the theoretical model to dissolve both analytes.

The results of the solubility assessment for both analytes are summarized in Table S.1 (see the Supporting Information). The solubility domains of SPMA and Ebe830 were plotted in the 3D Hansen space according to the experimentally determined HSP values and R_0 (Figure 1). It was considered that the potentially good solvents to dissolve both SPMA and Ebe830 should be inside the overlap of the solubility domains of the solutes. To find the suitable solvent candidates from the database of solvents, the HSP coordinates of the middle point of the overlap were determined. The RED from the middle point of the overlap were calculated (eq 3) for ca. 1300 solvents with known HSP parameters.[28] The potential solvent candidates were listed and ranked according to increasing distance from said midpoint (Table S.2, Supporting Information). The 48 solvents from Table S.2 were screened against the following criteria in order to find the potential solvent for membrane formulation components. The optimal solvent for membrane fabrication should be nontoxic, low cost, and easily accessible on the market. Moreover, it should represent the non-UV-reactive class of solvents as an alternative for UV-reactive AA. Most of the shortlisted solvents were rejected because of their acute toxicity or mutagenicity. The use of harmful solvents in the membrane fabrication process causes a serious threat to human health and the environment, implying ethical and economic consequences that would make industrialization of the fabrication process impossible. The second large group of solvents from the shortlist was excluded based on the market price and availability. Solvent share in the membrane liquid formulation is generally high (reaching 25% in the case of AA formulation), which can result in a remarkable price elevation of the final product when expensive solvents are used. The use of less common solvents causes an additional concern in constituting a bottleneck in the supply chain. Ethyl lactate, dipropylene glycol, and acetic acid comply with all above requirements and were used for membrane fabrication.

3.2. Membrane Fabrication. The solubility of SPMA in the solvents selected for membrane fabrication was assessed. The SPMA-solvent ratio in each formulation was defined by the maximum solubility of SPMA in a given solvent allowing one to obtain a homogeneous and stable mixture. The highest load of SPMA was achieved with the use of acetic acid (30% w/w). Solubility of SPMA in ethyl lactate and dipropylene glycol allows it to reach only 5% w/w in the formulation in both cases. Four distinct hIEMs were formulated with selected solvents: acrylic acid (AA-hIEM), acetic acid (AcA-hIEM), dipropylene glycol (DPG-hIEM), and ethyl lactate (EtL-hIEM). The concentrations of the TPO photoinitiator and Ebecryl 830 (Ebe830) resin were kept constant for all formulations. PVP was added to the EtL-hIEM formulation to increase the viscosity and prevent soaking of the formulation into the PVC-silica substrate (Figure 2). All formulations

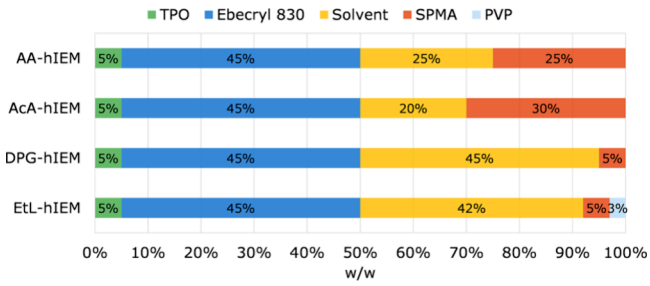

Figure 2. Detailed composition of the formulations of hIEMs. Solvent refers to a specific solvent used to prepare the given hIEM formulation: AA-hIEM, AcA-hIEM, DPG-hIEM, and EtL-hIEM.

remain a clear and homogeneous mixture throughout the fabrication process of the membranes. The acidic solvents may cause potential degradation of membrane formulation precursors since SPMA and Ebe830 contain ester bonds. The background studies show that extension of the formulation mixing time, resulting in a longer contact of unreacted monomers with acidic solvents, has no significant impact on the performance of the membranes. Thus, the membrane fabrication time is considered too short to observe significant degradation of the formulation. Each membrane formulation was prepared and coated on the PVC-silica support according to the procedure described in section 2.4. The detailed composition of each membrane formulation is reported in Figure 2.

https://doi.org/10.1021/acs.iecr.3c02174
Ind. Eng. Chem. Res. XXXX, XXX, XXX−XXX

The estimated cost of fabrication of each hIEM does not exceed 100 €/m^2, which is significantly lower than the cost of commercially available membrane standards. The details of the cost estimation calculation for fabricated hIEMs are available in the Supporting Information.

The thicknesses of the membranes and membrane- coating layers were evaluated using an optical microscope (VHX-7000 Keyence, Japan) and are summarized in Table 1.

Table 1. Thickness of the hIEM Functional Coatings and the Overall Membrane Thickness of hIEMs and Commercial Benchmarks

membrane	membrane thickness [μm]	coating thickness [μm]
PVC-SiO_2 substrate	332 ± 15	-
AA-hIEM	374 ± 14	38.5 ± 5.7
AcA-hIEM	380 ± 18	45.5 ± 7.1
DPG-hIEM	381 ± 9	39.7 ± 5.7
EtL-hIEM	369 ± 12	38.2 ± 6.1
Nafion 117	181 ± 4	-
CMHPES	311 ± 11	-
FKS-PET-75	79 ± 6	-

The membranes were soaked in 0.5 M NaCl solution for 48 h, and the deformational behavior was observed (Figure 3). It was observed that membranes prepared with the use of ethyl lactate, DPG, and AcA remain flatter after soaking in the electrolyte than the membrane prepared with AA. This improves the handleability and minimizes the risk of extensive deformation and breaking of the membrane during mounting and operation, for example, in an ED stack.[47]

The positive influence on the overall handleability of these membranes in a wet state is mostly due to the higher flexibility and lower degree of mechanical deformation in comparison to the membrane fabricated using AA. The EtL and DPG membrane variants show almost no difference in shape between the dry and wet forms. In the case of EtL-hIEM, the polymerization shrinkage of the coating during UV curing was not counterbalanced by the opposing effect of swelling of the coating after contact with the electrolyte. Thus, EtL-hIEM remains deformed in the opposite direction than the other hIEMs after soaking in the electrolyte. The AcA-hIEM reveals only a slight deformation upon wetting. This indicates that the swelling of functional coatings prepared with non-UV-reactive solvents is much less severe than for the AA-hIEM. Since the low swelling in the case of DPG-hIEM and EtL-hIEM can be partially explained by the relatively low concentration of functional sulfonic groups in the formulation, the crucial role of the solvent in limiting the curling of the membrane is clearly visible in the case of the AcA-hIEM. Despite having the highest content of sulfonic groups, the AcA-hIEM does not show excessive mechanical deformation (Figure 3). The reason for this is the relatively low volumetric expansion of the coating of AcA-hIEM due to more loose ionomer structure and preswollen active groups within the polymeric network. The greatly improved handleability of AcA-hIEM, due to less severe deformation, is granted with transport performance in line with the AA-hIEM. The assessment of the mechanical properties of hIEMs is given in the Supporting Information. Results of the mechanical testing of hIEMs were benchmarked against commercial standard membranes and are summarized in Table S.3.

3.3. WU and IEC. The IEC and WU are interdependent parameters having an influence on the water and ion transport through the membrane. A high IEC is crucial for maintaining high effectiveness in the transport of counterions while improving the membrane selectivity by repelling the coions. A high WU promotes nonselective transport of both charged species as well as inert molecules.[10] The WU and IEC were determined only for the membrane ionomer coatings (without

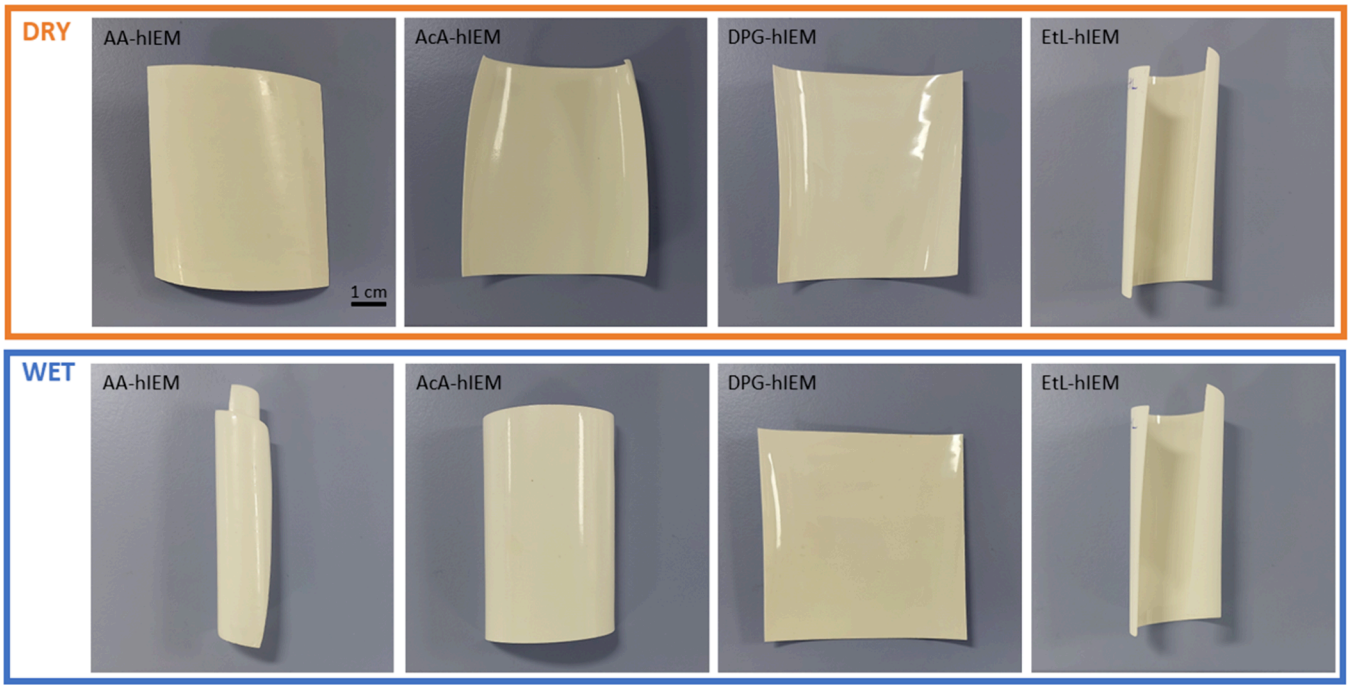

Figure 3. Photograph showing mechanical behavior of fabricated hIEMs. It depicts a sheet of each fabricated hIEM before (dry) and after soaking in an electrolyte (wet).

https://doi.org/10.1021/acs.iecr.3c02174
Ind. Eng. Chem. Res. XXXX, XXX, XXX−XXX

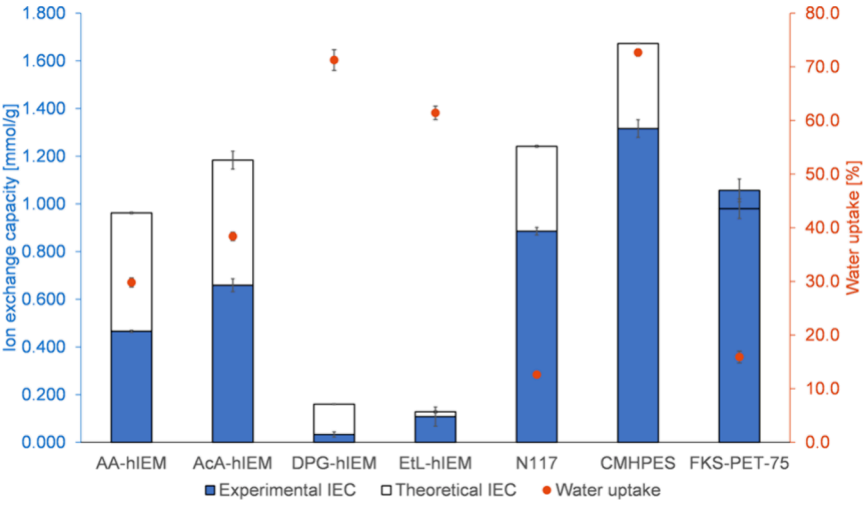

Figure 4. IEC and WU of hIEMs and commercial membranes.

the substrate present). The reason for this is that the coating is an effective functional ion-exchange layer. Acetic acid allows to reach the highest IEC (0.659 mmol·g^{-1}) among the non-UV-reactive solvents (0.033 mmol·g^{-1} for DPG and 0.108 mmol·g^{-1} for EtL formulation), and it is significantly higher than the IEC obtained for formulation prepared with AA (0.466 mmol·g^{-1}) (Figure 4). The experimental IEC (IEC_{EXP}) were compared with the theoretical IEC (IEC_{TH}) calculated based on the sulfur content (Section 2.6) in the coating material (eq 13).

$$IEC_{TH} = \frac{C_s \times 1000}{M_s} \tag{13}$$

where C_s is the sulfur content in the sample [%] and M_s is the molar mass of sulfur.

The experimental IEC values are lower than the calculated theoretical IEC values for each coating material. There are two possible explanations for this. First, the highly cross-linked structure of the ionomer forms a steric hindrance and limits the accessibility of the functional charged groups for the counterions. Second, poor incorporation of the sulfonic monomer into the ionomer structure can lead to loss of some of the functional molecules. Low IEC values for DPG and EtL coating materials can be associated with the low concentration of the functional monomer used in these formulations. Additionally, the experimentally recorded IEC of DPG-hIEM reaches only 20.6% of the theoretical IEC value for this membrane. This indicates that despite the high WU observed for the DPG-hIEM (71.3% mass), many ionic sites remain inactive in the membrane. That is despite the expectation that high WU generally improves the accessibility of charged groups. The exceptionally low IEC of DPG-hIEM and EtL-hIEM could not facilitate efficient ion transport through the membrane. This was confirmed by observing a very high resistivity of these membranes discussed in Section 3.4. The measured high water content in the case of DPG-hIEM and EtL-hIEM is a result of both solvation of ion-exchange groups in the polymer structure and replacement of the unreacted solvent by the electrolyte. The presence of free water in the ionomer structure can significantly contribute to the apparent WU and compromise the membrane selectivity.

Among the fabricated hIEMs, the experimentally determined IEC in relation to the theoretical IEC is the highest for EtL formulation (84.4%), while the WU of EtL formulation reaches 61.4%. The experimental IEC of AcA-hIEM is lower than that of the commercial benchmark materials (Figure 4). However, the theoretical IEC of AcA-hIEM, almost as high as the IEC of Nafion 117, introduces a margin for potential improvement of the effective IEC, for example, increasing the accessibility of functional groups by optimization of the fabrication process. Interestingly, the IEC_{EXP} value obtained for FKS-PET-75 was slightly higher than the theoretical IEC. This discrepancy is most probably due to the relatively high standard deviation of IEC_{EXP}, and it can be assumed that the IEC_{EXP} equals IEC_{TH}. This indicates that all functional groups in FKS-PET-75 were accessible and were involved in the ion exchange. The IEC_{EXP} values for Nafion 117 and CMHPES reached 71.3 and 78.7% of the theoretical IEC, respectively.

3.4. ASR and Selectivity. ASR measurements were performed for all fabricated hIEMs. The resistivity of EtL-hIEM and DPG-hIEM membranes was very high, and obtaining reproducible results within the ASR range of AA-hIEM and AcA-hIEM was not possible. Thus, EtL-hIEM and DPG-hIEM were considered not conductive enough and were not used for further testing. The ASR of bare PVC-silica substrate was 3.65 Ω·cm^{-2}. The ASR and selectivity of the AA-hIEM and AcA-hIEM membranes and commercial reference membranes are presented in Figure 5. The AcA-hIEM shows an improved ASR (6.43 Ω·cm^{-2}) over that of the AA-hIEM (12.1 Ω·cm^{-2}). An improvement in the ASR for the AcA-hIEM was achieved as a result of the higher effective IEC and higher WU when compared with the AA-hIEM. The ASR for AcA-hIEM is also significantly lower than that of the commercial Ralex CMHPES membrane (8.11 Ω·cm^{-2}) (Figure 5).

Considering that the supporting layer is introducing a substantial share to the hIEM resistivity, subtracting the bare supporting layer resistance results in 2.78 and 8.45 Ω·cm^{-2} resistance of ion-exchange coating for AcA-hIEM and AA-hIEM, respectively. This means that the net resistivity of the ion-exchange layer was reduced by 67.1% while using acetic acid in the membrane formulation. The substantial improvement in the ionomer coating resistivity is relevant as it is not the layer of a high resistance of the membrane sheet, constituting 43.2% to the overall membrane resistance in case of AcA-hIEM, while in case of AA-hIEM, the ionomer coating share is 69.8%. Further study focused on lowering the

https://doi.org/10.1021/acs.iecr.3c02174
Ind. Eng. Chem. Res. XXXX, XXX, XXX−XXX

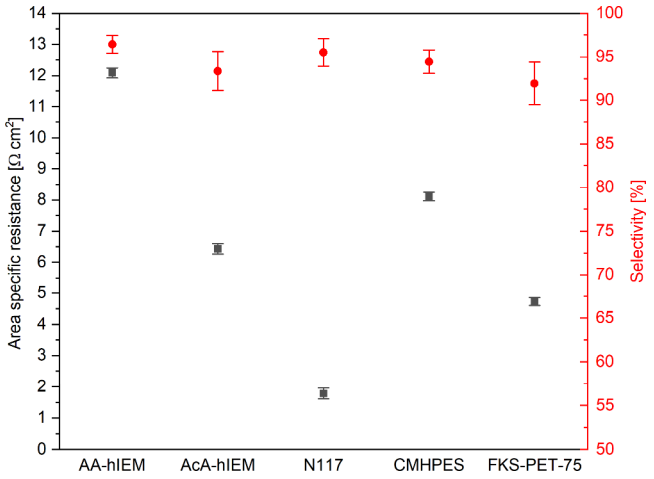

Figure 5. ASR and selectivity of hIEMs and commercial membranes.

resistance of a supporting layer may be performed, potentially allowing to reduce the membrane resistivity closer to the resistivity of FKS-PET-75 or Nafion 117. The relatively low resistivity of the AcA-hIEM makes it suitable for use in applications such as organic redox flow batteries in which the efficiencies strongly depend on the resistance of the system. The potential utilization of developed hIEMs should be considered for organic RFBs employing nonharsh aqueous solutions due to potential low stability of the membranes under highly acidic conditions. Unfortunately, the higher WU of AcA-hIEM is most probably a reason of a compromised selectivity of the membrane (93.4% for AcA-hIEM and 96.4% for AA-hIEM, respectively). Due to its moderate selectivity, the AcA-hIEM membrane is less attractive for applications such as electrodialysis in which high selectivity is of high importance. However, the selectivity of AcA-hIEM can be considered sufficiently high, which is clear when compared to the selectivity of reference membranes: Nafion 117 (95.5%), CMHPES (94.5%), and FKS-PET-75 (92.0%).

3.5. Permeability of Ethanol and Osmotic Water Transport. While the transport performance of the membrane toward charged molecules can be somehow assessed by the determination of ASR and selectivity, it does not give any information about the transport of neutral species. The migration of uncharged molecules through the membrane is a phenomenon of interest for numerous membrane applications. Transport properties of light charge-neutral organic molecules through the membrane can have a significant impact on the efficiency of the system in applications such as organic redox flow batteries and artificial photosynthesis cells.[48−50] The membrane-transport properties toward neutral species were assessed by means of ethanol permeability. Ethanol is a molecule of high importance in many membrane systems and can be considered as a model organic molecule for permeability tests.

According to the discussion in previous sections, the higher WU of AcA-hIEM over the AA-hIEM membrane promotes the transport of uncharged molecules, which manifests in a slightly higher ethanol crossover through AcA-hIEM (Figure 6). However, WU is not the only parameter determining the migration of uncharged species across the membrane. The Nafion 117 membrane shows a high WPC (2.4×10^{-3} $cm^4 \cdot s^{-1} \cdot mol^{-1}$) and permeability of ethanol (8.3×10^{-4} $cm \cdot min^{-1}$) related to its low WU (12.6%). The ethanol permeability for AcA-hIEM (1.2×10^{-4} $cm \cdot min^{-1}$) is lower than those for CMHPES (1.6×10^{-4} $cm \cdot min^{-1}$) and Nafion 117 benchmark membranes (Figure 6).

The higher content of free water in the AcA-hIEM compared to that in the AA-hIEM results in both a higher WPC and ethanol permeability. IEMs based on perfluorinated sulfonic acid ionomers such as Nafion, despite their high stability and good conductivity, have certain limitations for application in, for example, artificial photosynthesis cells due to the high permeability of light alcohols. Thus, the advantageous ethanol permeability of AcA-hIEM makes it a potential good alternative for Nafion in systems where a low ethanol crossover is highly desirable.

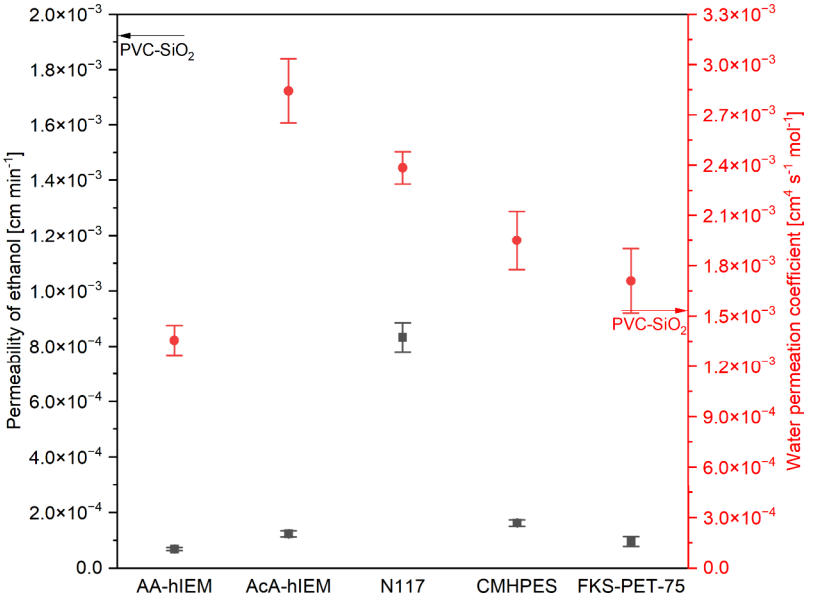

Figure 6. Ethanol permeability parameter and WPC of hIEMs and commercial membranes.

https://doi.org/10.1021/acs.iecr.3c02174
Ind. Eng. Chem. Res. XXXX, XXX, XXX−XXX

4. CONCLUSIONS

It was proven that a substantial improvement in hindering the membrane mechanical deformation can be done by the introduction of the non-UV-reactive solvent in the ionomer precursor liquid formulation. The membrane mechanical behavior was improved while retaining transport properties on the levels of industrial standard cation-exchange membranes. This is expected to facilitate membrane system assembly and mitigate the risk of operational failure. The developed AcA-hIEM due to its good mechanical properties and competitive performance at significantly lower cost can potentially be a cost-effective alternative for commercial cation-exchange membranes. Acetic acid was selected utilizing Hansen solubility theory as the optimal non-UV-reactive solvent to compatibilize 3-sulfopropyl methacrylate and Ebecryl 830 into a liquid formulation. The formulation of mechanically stable membranes with the use of acetic acid complies with the sustainable fabrication process of hIEMs. Thus, the fabrication of low-cost AcA-hIEM in a limited waste generation process creates the potential to use such membrane materials in various applications, lowering the total capital and environmental cost. HST can be utilized to search for other formulation components and additives to tune the membrane properties. Acetic acid allows one to reach a high content of SPMA functional monomer (30% w/w) in an ionomer precursor formulation, which translates to a high IEC (0.659 mmol/g). It was proven that AcA-hIEM offers a good ionic conductivity (6.43 $\Omega \cdot cm^{-2}$) with high selectivity (93.4%) compared to commercial benchmark membranes. The membrane fabricated with acetic acid shows improved mechanical properties and handleability over the AA membrane preparation.

■ ASSOCIATED CONTENT

Supporting Information

The Supporting Information is available free of charge at https://pubs.acs.org/doi/10.1021/acs.iecr.3c02174.

Results of Hansen solubility determination of SPMA and Ebecryl 830 in screening solvents; list of potential solvents for SPMA and Ebecryl 830 identified utilizing HST; description of the method of tensile strength determination and results of mechanical testing of membranes; images of the cross-section of fabricated hIEMs; cost estimation of membrane fabrication; and calculation of junction potential (PDF)

■ AUTHOR INFORMATION

Corresponding Author

Daniel Firganek − *Amer-Sil S.A., L-8281 Kehlen, Luxembourg; Department of Chemical Engineering, KU Leuven, B-3001 Leuven, Belgium;* orcid.org/0000-0002-8870-2714; Email: Daniel.Firganek@amer-sil.com

Authors

Mateusz L. Donten − *Amer-Sil S.A., L-8281 Kehlen, Luxembourg*

Bart Van der Bruggen − *Department of Chemical Engineering, KU Leuven, B-3001 Leuven, Belgium*

Complete contact information is available at: https://pubs.acs.org/10.1021/acs.iecr.3c02174

Author Contributions

D.F.: Conceptualization, methodology, investigation, software, visualization, and writing−original draft. M.L.D.: Conceptualization, methodology, supervision, writing−review, and editing. B.V.: Conceptualization, methodology, supervision, writing−review, and editing. The manuscript was written through contributions of all authors. All authors have given approval to the final version of the manuscript.

Notes

The authors declare no competing financial interest.

■ ACKNOWLEDGMENTS

Research carried out under HYSOLCHEM: This project has received funding from the European Union's Horizon 2020 research and innovation programme under grant agreement no. 101017928.

■ ABBREVIATIONS

AA-hIEM: hierarchical ion-exchange membrane prepared with acrylic acid
AcA-hIEM: hierarchical ion-exchange membrane prepared with acetic acid
DPG-hIEM: hierarchical ion-exchange membrane prepared with dipropylene glycol
EtL-hIEM: hierarchical ion-exchange membrane prepared with ethyl lactate
AA: acrylic acid
AcA: acetic acid
DPG: dipropylene glycol
EtL: ethyl lactate
SPMA: 3-sulfopropyl methacrylate potassium salt
Ebe830: Ebecryl 830
TPO: diphenyl(2,4,6-trimethylbenzoyl) phosphine oxide
PVP: polyvinylpyrrolidone
DMSO: dimethylsulfoxide
NMP: *N*-Methyl-2-pyrrolidone
DVB: divinylbenzene
THF: tetrahydrofuran
DMAC: N,N-dimethylacetamide
DMF: dimethylformamide
PVC: polyvinyl chloride
IEM: ion exchange membrane
hIEM: hierarchical ion exchange membrane
ED: electrodialysis
HSP: Hansen solubility parameters
RED: relative energy distance
WU: water uptake
IEC: ion exchange capacity
ASR: area specific resistance
PTFE: polytetrafluoroetylene
UV: Ultraviolet

■ REFERENCES

(1) Dobyns, B. M.; Kim, J. M.; Beckingham, B. S. Multicomponent Transport of Methanol and Sodium Acetate in Poly(Ethylene Glycol) Diacrylate Membranes of Varied Fractional Free Volume. *Eur. Polym. J.* **2020**, *134*, No. 109809.

(2) Drioli, E.; Curcio, E. Membrane Engineering for Process Intensification: A Perspective. *J. Chem. Technol. Biotechnol.* **2007**, *82* (3), 223−227.

(3) Jiang, S.; Sun, H.; Wang, H.; Ladewig, B. P.; Yao, Z. A Comprehensive Review on the Synthesis and Applications of Ion Exchange Membranes. *Chemosphere* **2021**, *282*, No. 130817.

(4) Zhao, W.-Y.; Zhou, M.; Yan, B.; Sun, X.; Liu, Y.; Wang, Y.; Xu, T.; Zhang, Y. Waste Conversion and Resource Recovery from Wastewater by Ion Exchange Membranes: State-of-the-Art and Perspective. *Ind. Eng. Chem. Res.* **2018**, *57* (18), 6025−6039.
(5) Conductive Membrane Coatings for High-Rate Vanadium Redox Flow Batteries | ACS Omega. https://pubs-acs-org.kuleuven.e-bronnen.be/doi/10.1021/acsomega.7b01787.
(6) Peighambardoust, S. J.; Rowshanzamir, S.; Amjadi, M. Review of the Proton Exchange Membranes for Fuel Cell Applications. *Int. J. Hydrogen Energy* **2010**, *35* (17), 9349−9384.
(7) Chabi, S.; Papadantonakis, K. M.; Lewis, N. S.; Freund, M. S. Membranes for Artificial Photosynthesis. *Energy Environ. Sci.* **2017**, *10* (6), 1320−1338.
(8) Ke, Y.; Yuan, W.; Zhou, F.; Guo, W.; Li, J.; Zhuang, Z.; Su, X.; Lu, B.; Zhao, Y.; Tang, Y.; Chen, Y.; Song, J. A Critical Review on Surface-Pattern Engineering of Nafion Membrane for Fuel Cell Applications. *Renewable Sustainable Energy Rev.* **2021**, *145*, No. 110860.
(9) Luo, Q.; Zhang, H.; Chen, J.; Qian, P.; Zhai, Y. Modification of Nafion Membrane Using Interfacial Polymerization for Vanadium Redox Flow Battery Applications. *J. Membr. Sci.* **2008**, *311* (1), 98−103.
(10) Klaysom, C.; Ladewig, B. P.; Lu, G. Q. M.; Wang, L. Preparation and Characterization of Sulfonated Polyethersulfone for Cation-Exchange Membranes. *J. Membr. Sci.* **2011**, *368* (1), 48−53.
(11) Park, C. H.; Lee, C. H.; Guiver, M. D.; Lee, Y. M. Sulfonated Hydrocarbon Membranes for Medium-Temperature and Low-Humidity Proton Exchange Membrane Fuel Cells (PEMFCs). *Prog. Polym. Sci.* **2011**, *36* (11), 1443−1498.
(12) Yadav, P.; Ismail, N.; Essalhi, M.; Tysklind, M.; Athanassiadis, D.; Tavajohi, N. Assessment of the Environmental Impact of Polymeric Membrane Production. *J. Membr. Sci.* **2021**, *622*, No. 118987.
(13) Molau, G. E. Heterogeneous Ion-Exchange Membranes. *J. Membr. Sci.* **1981**, *8* (3), 309−330.
(14) Jashni, E.; Hosseini, S. M.; Shen, J. A New Approach to Providing Heterogeneous Cation-Exchange Membrane with Enhanced Electrochemical and Desalination Performance by Incorporation of Fe3O4/PVP Composite Nanoparticles. *Ionics* **2020**, *26* (2), 861−874.
(15) Bakangura, E.; Cheng, C.; Wu, L.; Ge, X.; Ran, J.; Khan, M. I.; Kamana, E.; Afsar, N.; Irfan, M.; Shehzad, A.; Xu, T. Hierarchically Structured Porous Anion Exchange Membranes Containing Zwetterionic Pores for Ion Separation. *J. Membr. Sci.* **2017**, *537*, 32−41.
(16) Deboli, F.; Van der Bruggen, B.; Donten, M. L. A Novel Concept of Hierarchical Cation Exchange Membrane Fabricated from Commodity Precursors through an Easily Scalable Process. *J. Membr. Sci.* **2021**, *636*, No. 119594.
(17) Charyton, M.; Iojoiu, C.; Fischer, P.; Henrion, G.; Etienne, M.; Donten, M. L. Composite Anion-Exchange Membrane Fabricated by UV Cross-Linking Vinyl Imidazolium Poly(Phenylene Oxide) with Polyacrylamides and Their Testing for Use in Redox Flow Batteries. *Membranes* **2021**, *11* (6), 436.
(18) Charyton, M.; Deboli, F.; Fischer, P.; Henrion, G.; Etienne, M.; Donten, M. L. Composite Anion Exchange Membranes Fabricated by Coating and UV Crosslinking of Low-Cost Precursors Tested in a Redox Flow Battery. *Polymers* **2021**, *13* (15), 2396.
(19) La Cerva, M.; Gurreri, L.; Tedesco, M.; Cipollina, A.; Ciofalo, M.; Tamburini, A.; Micale, G. Determination of Limiting Current Density and Current Efficiency in Electrodialysis Units. *Desalination* **2018**, *445*, 138−148.
(20) Ionomer-coated filtration membranes as an alternative to ion-exchange membranes for demineralization by electrodialysis - Kadel - 2022 - Journal of Polymer Science - Wiley Online Library. https://onlinelibrary-wiley-com.kuleuven.e-bronnen.be/doi/10.1002/pol.20210452 (accessed 20 Dec, 2022).
(21) Stenina, I.; Golubenko, D.; Nikonenko, V.; Yaroslavtsev, A. Selectivity of Transport Processes in Ion-Exchange Membranes: Relationship with the Structure and Methods for Its Improvement. *Int. J. Mol. Sci.* **2020**, *21* (15), 5517.
(22) Li, F.; Larock, R. C. Synthesis, Structure and Properties of New Tung Oil−Styrene−Divinylbenzene Copolymers Prepared by Thermal Polymerization. *Biomacromolecules* **2003**, *4* (4), 1018−1025.
(23) Deboli, F.; Van der Bruggen, B.; Donten, M. L. A Versatile Chemistry Platform for the Fabrication of Cost-Effective Hierarchical Cation and Anion Exchange Membranes. *Desalination* **2022**, *535*, No. 115794.
(24) Bakangura, E.; Cheng, C.; Wu, L.; Ge, X.; Ran, J.; Khan, M. I.; Kamana, E.; Afsar, N.; Irfan, M.; Shehzad, A.; Xu, T. Hierarchically Structured Porous Anion Exchange Membranes Containing Zwetterionic Pores for Ion Separation. *J. Membr. Sci.* **2017**, *537*, 32−41.
(25) Kononenko, N.; Nikonenko, V.; Grande, D.; Larchet, C.; Dammak, L.; Fomenko, M.; Volfkovich, Yu. Porous Structure of Ion Exchange Membranes Investigated by Various Techniques. *Adv. Colloid Interface Sci.* **2017**, *246*, 196−216.
(26) Saunier, J.; Alloin, F.; Sanchez, J. Y.; Maniguet, L. Plasticized Microporous Poly(Vinylidene Fluoride) Separators for Lithium-Ion Batteries. III. Gel Properties and Irreversible Modifications of Poly(Vinylidene Fluoride) Membranes under Swelling in Liquid Electrolytes. *J. Polym. Sci., Part B: Polym. Phys.* **2004**, *42* (12), 2308−2317.
(27) Venkatram, S.; Kim, C.; Chandrasekaran, A.; Ramprasad, R. Critical Assessment of the Hildebrand and Hansen Solubility Parameters for Polymers. *J. Chem. Inf. Model.* **2019**, *59* (10), 4188−4194.
(28) Hansen, C. M. *Hansen Solubility Parameters: A User's Handbook*, 2nd ed.; CRC Press: Boca Raton, 2007.
(29) Rasool, M. A.; Pescarmona, P. P.; Vankelecom, I. F. J. Applicability of Organic Carbonates as Green Solvents for Membrane Preparation. *ACS Sustainable Chem. Eng.* **2019**, *7* (16), 13774−13785.
(30) Lee, C. H.; Park, H. B.; Chung, Y. S.; Lee, Y. M.; Freeman, B. D. Water Sorption, Proton Conduction, and Methanol Permeation Properties of Sulfonated Polyimide Membranes Cross-Linked with N,N-Bis(2-Hydroxyethyl)-2-Aminoethanesulfonic Acid (BES). *Macromolecules* **2006**, *39* (2), 755−764.
(31) Yang, D.; Yu, H.; Li, G.; Zhao, Y.; Liu, Y.; Zhang, C.; Song, W.; Shao, Z. Fine Microstructure of High Performance Electrode in Alkaline Anion Exchange Membrane Fuel Cells. *J. Power Sources* **2014**, *267*, 39−47.
(32) Wang, C.; He, Z.; Xie, X.; Mai, X.; Li, Y.; Li, T.; Zhao, M.; Yan, C.; Liu, H.; Wujcik, E. K.; Guo, Z. Controllable Cross-Linking Anion Exchange Membranes with Excellent Mechanical and Thermal Properties. *Macromol. Mater. Eng.* **2018**, *303* (3), No. 1700462.
(33) Yoon, J.; Kwon, H. J.; Kang, S.; Brack, E.; Han, J. Portable Seawater Desalination System for Generating Drinkable Water in Remote Locations. *Environ. Sci. Technol.* **2022**, *56* (10), 6733−6743.
(34) Tian, C.; Kristiansen, K. R.; Kjelstrup, S.; Barragán, V. M. Two Methods for Determination of Transport Numbers in Ion-Exchange Membranes. *Int. J. Thermophys* **2022**, *43* (1), 14.
(35) Berezina, N. P.; Timofeev, S. V.; Rollet, A.-L.; Fedorovich, N. V.; Durand-Vidal, S. Transport−Structural Parameters of Perfluorinated Membranes Nafion-117 and MF-4SK. *Russ. J. Electrochem.* **2002**, *38* (8), 903−909.
(36) de los Ríos, M. D.; Ramos, E. H. Determination of the Hansen Solubility Parameters and the Hansen Sphere Radius with the Aid of the Solver Add-in of Microsoft Excel. *SN Appl. Sci.* **2020**, *2* (4), 2512.
(37) Wilhelm, F. G.; Pünt, I. G. M.; van der Vegt, N. F. A.; Strathmann, H.; Wessling, M. Cation permeable membranes from blends of sulfonated poly(ether ether ketone) and poly(ether sulfone). *J. Membr. Sci.* **2002**, *199* (1−2), 167−176.
(38) Długołęcki, P.; Nymeijer, K.; Metz, S.; Wessling, M. Current Status of Ion Exchange Membranes for Power Generation from Salinity Gradients. *J. Membr. Sci.* **2008**, *319* (1), 214−222.
(39) Cha, J.-E.; Seo, M. H.; Choi, Y.-W.; Kim, W. B. A Practical Approach to Measuring the Ion-Transport Number of Cation-Exchange Membranes: Effects of Junction Potential and Analyte Concentration. *J. Membr. Sci.* **2021**, *635*, No. 119471.

https://doi.org/10.1021/acs.iecr.3c02174
Ind. Eng. Chem. Res. XXXX, XXX, XXX−XXX

(40) Kingsbury, R. S.; Flotron, S.; Zhu, S.; Call, D. F.; Coronell, O. Junction Potentials Bias Measurements of Ion Exchange Membrane Permselectivity. *Environ. Sci. Technol.* **2018**, *52* (8), 4929−4936.
(41) Ji, Y.; Geise, G. M. The Role of Experimental Factors in Membrane Permselectivity Measurements. *Ind. Eng. Chem. Res.* **2017**, *56* (26), 7559−7566.
(42) Güler, E.; Elizen, R.; Vermaas, D. A.; Saakes, M.; Nijmeijer, K. Performance-Determining Membrane Properties in Reverse Electrodialysis. *J. Membr. Sci.* **2013**, *446*, 266−276.
(43) Mali, Z.; Chen, X.; Pan, J.; Yang, S.; Han, B.; Xue, L.; Shen, J.; Gao, C.; Van der Bruggen, B. A novel UV-crosslinked sulphonated polysulfone cation exchange membrane with improved dimensional stability for electrodialysis. *Desalination* **2017**, *415*, 29−39.
(44) Luo, T.; Abdu, S.; Wessling, M. Selectivity of ion exchange membranes: A review. *J. Membr. Sci.* **2018**, *555*, 429−454.
(45) Geise, G. M.; Hickner, M. A.; Logan, B. E. Ionic Resistance and Permselectivity Tradeoffs in Anion Exchange Membranes. *ACS Appl. Mater. Interfaces* **2013**, *5* (20), 10294−10301.
(46) Tanaka, Y. 2 - Fundamental Properties of Ion Exchange Membranes. In *Ion Exchange Membranes (Second ed.)*; Tanaka, Y., Ed.; Elsevier: Amsterdam, 2015; pp 29−65.
(47) Battaglia, G.; Gurreri, L.; Airò Farulla, G.; Cipollina, A.; Pirrotta, A.; Micale, G.; Ciofalo, M. Membrane Deformation and Its Effects on Flow and Mass Transfer in the Electromembrane Processes. *Int. J. Mol. Sci.* **2019**, *20* (8), 1840.
(48) McCormack, P. M.; Koenig, G. M.; Geise, G. M. Thermodynamic Interactions as a Descriptor of Cross-Over in Nonaqueous Redox Flow Battery Membranes. *ACS Appl. Mater. Interfaces* **2021**, *13* (41), 49331−49339.
(49) Dischinger, S. M.; Gupta, S.; Carter, B. M.; Miller, D. J. Transport of Neutral and Charged Solutes in Imidazolium-Functionalized Poly(Phenylene Oxide) Membranes for Artificial Photosynthesis. *Ind. Eng. Chem. Res.* **2020**, *59* (12), 5257−5266.
(50) Song, S.; Tsiakaras, P. Recent Progress in Direct Ethanol Proton Exchange Membrane Fuel Cells (DE-PEMFCs). *Appl. Catal., B* **2006**, *63* (3), 187−193.

https://doi.org/10.1021/acs.iecr.3c02174
Ind. Eng. Chem. Res. XXXX, XXX, XXX−XXX